Low Temperature Synthesis of α-Fe$_2$O$_3$ Nano-rods Using Simple Chemical Route

Majid Farahmandjou[*] **, Farzaneh Soflaee**
Department of Physics, Collage of Science, Varamin Pishva Branch, Islamic Azad University, Varamin, Iran

Abstract

Iron oxide (Fe$_2$O$_3$) is widely used as a catalyst, pigment and gas sensitive material. In this article, α-Fe$_2$O$_3$ nano-rods were first synthesized via a simple chemical method using iron(III) nitrate 9-hydrate (Fe(NO$_3$)$_3$.9H$_2$O) as precursor. XRD pattern showed that the iron oxide nanoparticles exhibited alpha-Fe$_2$O$_3$ (hematite) structure in nanocrystals. The single-phase α- Fe$_2$O$_3$ nano-rods were prepared when the samples calcined at 500 °C. The smallest particle size was found to be 18 nm in diameter. The SEM studies depicted rod-like shaped particles with formation of clusters by increasing annealing temperature. The sharp peaks in FTIR spectrum determined the purity of Fe$_2$O$_3$ nanoparticles and absorbance peak of UV-Vis spectrum showed the small bandgap energy of 2.77 ev. The VSM result showed a coercive field and saturation magnetism around 90 G and 9.95 emu/g, respectively.

1. Introduction

In the past decade, magnetic nanomaterials have attracted much attention due to their physical properties and technological applications [1–3]. Nanoparticles of iron oxide, in its different phases, are being currently explored for their diverse range of applications such as magnetic storage media, environment protection, sensors, catalysis, clinical diagnosis and treatment etc.

The attention which is being focused on their synthesis and characterization is well-deserved as

they have the capability to exhibit certain superior properties as compared to bulk. In many cases nanocrystalline iron oxide can enhance materials performance or improve industrial processing. Iron oxide (Fe$_2$O$_3$) is an important semiconductor for the study of polymorphism and the magnetic and structural phase transitions of nanoparticles.

In the past, nanostructures of iron oxides such as α- Fe$_2$O$_3$, γ- Fe$_2$O$_3$, β- Fe$_2$O$_3$ and Fe$_3$O$_4$, have evoked remarkable interest from both theoretical and experimental point of view because of their

potential applications in nanodevices [4]. The phase transformation which occurs during calcination gives rise to transform α- Fe_2O_3 powder which has undergone considerable aggregation and grain growth [5,6]. Gamma and epsilon type Fe_2O_3 are ferromagnetic; alpha Fe_2O_3 is a canted antiferromagnetic while beta type Fe_2O_3 is a paramagnetic material. As alpha Fe_2O_3 has canted magnetism which means that the magnetic moments of the two magnetic sub-lattices do not fully cancel each other and results in small magnetic moment value in the direction of the basal plane. When the size of the magnetic particles becomes very small the magnetic moment in the domain fluctuates in direction, due to thermal agitation which leads to superparamagnetism. Among different magnetic nanoparticles, α- Fe_2O_3 is a very common magnetic material as it has potential applications in the chemical industry and also in drug delivery [7-9]. Alpha- Fe_2O_3 is also an environment friendly n-type semiconductor and thermodynamically most stable phase of iron oxide under ambient conditions. It can be used as catalyst, gas sensing material to detect combustible gases [10,11].

A lot of experiments have been carried out to make its use in composites for many useful applications [12,13]. A number of preparation techniques have been employed earlier for the preparation of Fe_2O_3 nanoparticles [14-18]. Some of them are very expensive and time consuming. In order to prepare homogenous nano-particles of iron oxide, researchers have employed in different routes to facilitate single-phase iron oxide nano-particles such as sol–gel processes [19], w/o microemulsion [20], combustion [21], solvothermal [22], hydrothermal [23], solvent evaporation and co-precipitation synthesis [25].

In this paper, ferric oxide nanorods were synthesized by chemical synthesis route using iron nitrate precursor. The samples were characterized by high resolution transmission electron microscopy (HRTEM), field effect scanning electron microscopy (FESEM) and X-ray diffraction (XRD), Fourier transform infrared spectroscopy (FTIR), UV-Vis spectrophotometer and vibration sampling magnetometer (VSM).

2. Experimental procedure

The starting chemicals used were iron (III) nitrate 9-hydrate (99.9%, Merck), ethanol (99.9%, Merck) without further purification. Distilled water was used as solvent. Precursor powders were synthesized using the following two methods. Firstly, 6 g of $Fe(NO_3)_3.9H_2O$ was dissolved in 150 mL distilled water with stirring at room temperature. A 12 mL ethanol solution was then added drop wise (drop rate= 1 mL min^{-1}) to the stirring mixture at room temperature. The Ph=1 was maintained during the synthesis. The resulting dark dispersion was continuously stirred for 1 h at room temperature and then heated to evaporate for 2 h at 80^0C to yield a black powder. The product were cooled to room temperature and finally calcined at 500^oC for 4 hours. For all samples, analyses were done without any washing and purification.

The specification of the size, structure and surface morphological properties of the as-synthesis and annealed Fe_2O_3 nanoparticles were carried out. X-ray diffractometer (XRD) was used to identify the crystalline phase and to estimate the crystalline size. The XRD pattern were recorded with 2θ in the range of

4-85° with type X-Pert Pro MPD, Cu-K$_\alpha$: λ = 1.54 Å. The morphology was characterized by field emission scanning electron microscopy (SEM) with type KYKY-EM3200, 25 kV and transmission electron microscopy (TEM) with type Zeiss EM-900, 80 kV.

3. Results and discussion

X-rar diffraction (XRD) at 40Kv was used to identify crystalline phases and to estimate the crystalline sizes.   Fig. 1 shows the X-ray diffraction patterns of the powder after heat treatment. A γ →α-Fe$_2$O$_3$ phase transformation took place during calcination between 300 and 400 ^{o}C. An abrupt increase in the amount of a phase occurred when the calcinations temperature incfrease above 400 ^{o}C. The α-Fe$_2$O$_3$ phase was the only phase present for the powder calcined above 500 ^{o}C. The exhibited picks correspond to the (012), (104), (110), (113), (024), (116), (018), (214) and (300) of a rhombohedral structure of α- Fe$_2$O$_3$ is identified using the standard data. The mean size of the ordered Fe$_2$O$_3$ nanoparticles has been estimated from full width at half maximum (FWHM) and Debye-Sherrer formula according to equation the following:

$$D = \frac{0.89\lambda}{B\cos\theta}$$

where, 0.89 is the shape factor, λ is the x-ray wavelength, B is the line broadening at half the maximum intensity (FWHM) in radians, and θ is the Bragg angle. The mean size of annealed single-phase α- Fe$_2$O$_3$ nanoparticles was around 18 nm from this Debye-Sherrer equation. The lattice constant so obtained for

alpha Fe$_2$O$_3$ nanoparticles were a=b=5.0342 A^o and c=13.74650 A^o.

The size and structure of nano α- Fe$_2$O$_3$ were evaluated using SEM analysis. These analyses show that high crystallinity emerged in the samples surface by increasing annealing temperature. With increasing temperature the morphology of the particles changes to the rod-like shaped and nanopowders were less agglomerate. Fig. 2(a) shows the SEM image of the as-prepared Fe$_2$O$_3$ nanoparticles. In this figure, the particles prepared with formation of clusters. Fig. 2(b) shows the SEM image of the annealed Fe$_2$O$_3$ nanoparticles at 500°C for 4 hours. The Fe$_2$O$_3$ nanocrystals formed were agglomerated. The rod-like shaped particles with clumped distributions are visible through the SEM analysis. The particle size of as-prepared Fe$_2$O$_3$ nanoparticles were measured about 20 nm and smallest crystallite size of annealed nanocrystals about 18 nm in diameter.
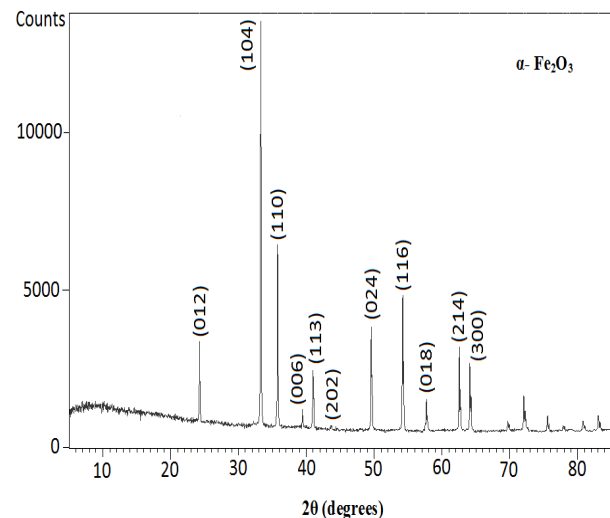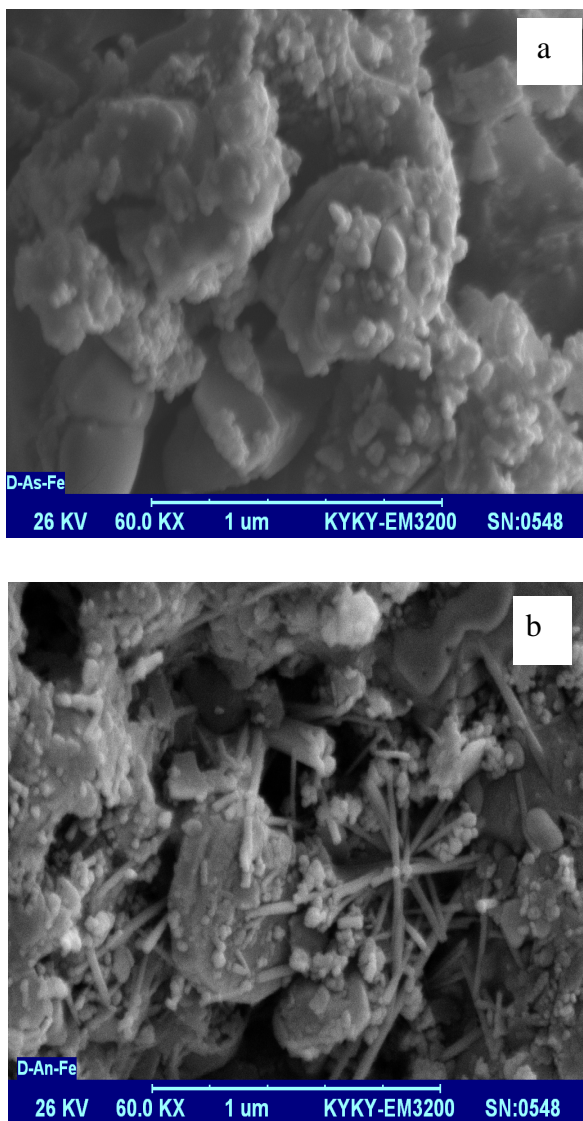

Fig. 1. XRD pattern of annealed sample.

Fig.2. SEM images of the Fe_2O_3 nanoparticles

Fig. 3. TEM image of as prepared Fe_2O_3 nanorode.

According to figure 4, the infrared spectrum (FTIR) of the synthesized Fe_2O_3 nanoparticles was in the range of 400-4000 cm^{-1} wavenumber which identify the chemical bonds as well as functional groups in the compound. The large broad band at 3398 cm^{-1} is ascribed to the O-H stretching vibration in O-H groups. The absorption picks around 1604 cm^{-1}, 1487 cm^{-1} are due to the asymmetric and symmetric bending vibration of C=O and absorption pick around 1293 cm^{-1} is ascribed to PVP group. The strong band below 700 cm^{-1} is assigned Fe-O stretching mode. The band corresponding to Fe-O stretching mode of Fe_2O_3 is seen at 576 cm^{-1}.

Fig.3 is the typical TEM of the as-synthesized Fe_2O_3 powder, from which it can be found that the sample contains nano- particles with mean particle size of 18 nm. The transmission electron microscopic analysis was carried out to confirm their growth pattern and the distribution of the crystallites. Figure shows the as-prepared TEM image of rod-like shaped Fe_2O_3 nanoparticles prepared by chemical route. It can be seen that nanorods were prepared with less aggregation.
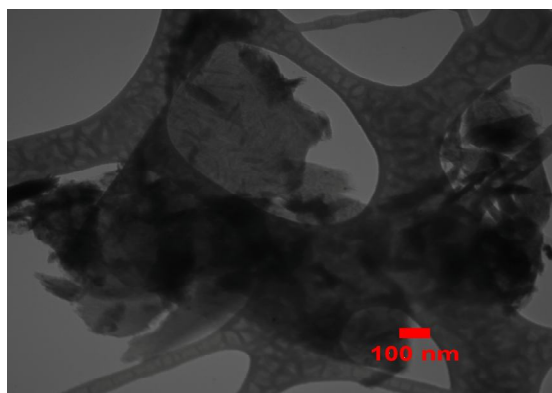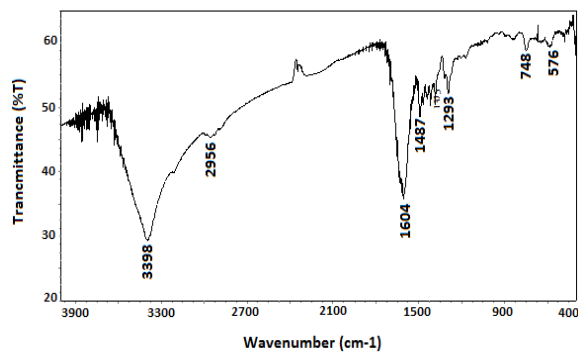

Fig. 4. FTIR spectrum of Fe_2O_3 sample.

UV-visible absorption spectral study may be assisted in understanding electronic structure of the optical band gap of the material. Absorption in the near ultraviolet region arises from electronic

transitions associated within the sample. UV–Vis absorption spectra of as-prepared and annealed Fe_2O_3 nanoparticles are shown in Figure 5. The strong absorption band at wavelength near 430 nm corresponds to small bandgap energy of 2.90 ev for as-synthesize Fe_2O_3 nanoparticles (Fig.5a). On the other hand the strong absorption band at wavelength near 450 nm corresponds to small bandgap energy of 2.77 ev for annealed Fe_2O_3 nanoparticles (Fig.5b). It is realized that by increasing annealing temperature the size of Fe_2O_3 nanoparticles decrease and the band gap energy decrease because of quantum effect.
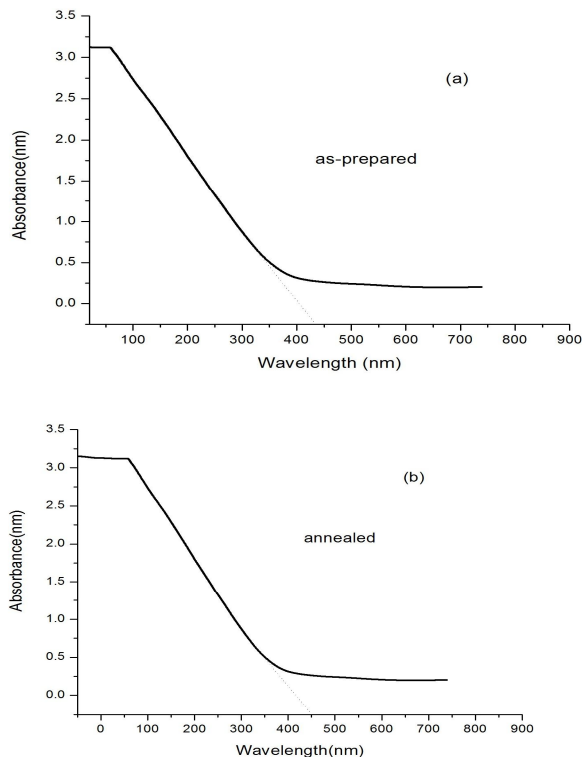

Fig. 5. spectra of Fe_2O_3 samples.

The classification of a material's magnetic property is based on magnetic susceptibility. Magnetizations M versus applied magnetic field H for powders of the samples are measured at room temperature by cycling the magnetic field between -20k to 20k G. The magnetization curve in Figure 6 shows hysteresis behavior in the low field region with the coercive field and saturation magnetism around 90 G and 9.95 emu/g, respectively.
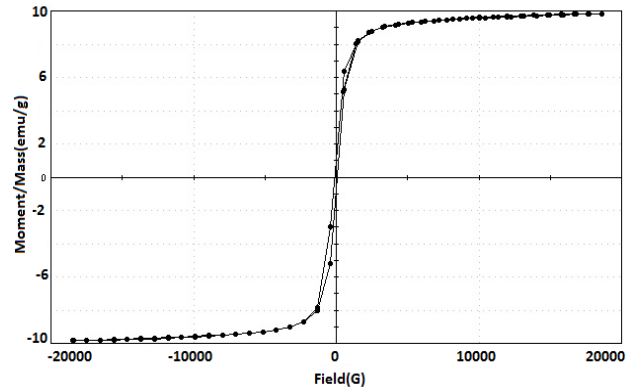

Fig. 6. Magnetic hysteresis loop of the Fe_2O_3 samples.

4. Conclusion

The α-Fe_2O_3 nano-rods were successfully synthesized by simple chemical method using ethanol solution of $Fe(NO_3)_3.9H_2O$. XRD spectrum shows rhombohedral (hexagonal) structure of α-Fe_2O_3. From SEM images, it is clear that with increasing temperature the morphology of the particles changes to rod-like shaped and nanopowders were less agglomerate. TEM image exhibits that the as-synthesized Fe_2O_3 nanorods with an average diameter about 18 nm with less aggregation. From the FTIR data, it is shown the presence of Fe-O stretching mode of Fe_2O_3. The UV–vis absorption analyses showed a strong absorption below 500 nm with a well-defined absorption peak at 480 nm, the direct small band gap is found to be 2.90 eV for as-prepared samples and 2.77 ev for annealed one. Magnetic measurements studies showed a good coercive field and saturation magnetism around 90 G and 9.95 emu/g respectively.

University for analysis and the discussions on the results.

References

[1] T. Whitney, P. Searson, J. Jiang, C. Chien, Science. 261 (1993) 1316-1319.

[2] D. Prodan, C. Chaneac, E. Tronc, J. Jolivet, R. Cherkaour, A. Ezzir, M. Nogues, J. Dormann, J. Magn. Magn. Mater. 203 (1999) 63-65.

[3] M. Morales, S. Veintemillas-Verdaguer, C. Serna, J. Mater. Res. 14 (1999) 3066-3072.

[4] W. Xinghong, L. Zhang, N. Yonghong, H. Jianming, C. Xiaofeng, J. Phys. Chem. C, 113 (2009) 7003-7008.

[5] W. Feitknecht, U. Mannweiler, Chim. Acta. 50 (1967) 570-581.

[6] H. El Ghandoor, H.M. Zidan, Mostafa M.H. Khalil, M.I.M. Ismail, Int. J. Electrochem. Sci., 7 (2012) 5734-5745 .

[7] N. Mimura, M. Takahara; Saito, T. Hattori, K. Ohkuma, M. Ando, Catalysis Today, 45 (1998) 61-64.

[8] Y.R. Uhm,W.W. Kim, C.K. Rhee, Scripta Materialia. 50 (2004) 561.-564.

[9] H.K. Edwards, E. Evans, S. McCaldin, P. Blood, D.H. Gregory, M. Poliakoff, J.Phys.: Conference Series. 26 (2006) 195-198.

[10] L. Huo, W. Li, L. Lu, Chem. Mater. 12 (2000) 790 -794.

[11] N. Koukabi, E. Kolvari, A. Khazaei, A.M. Zolfigol , S.B. Shaghasemi, Khavasi, H. Reza, Chem. Commun. 47 (2011) 9230.-9232.

[12] J. Zhang, X. Liu, L. Wang, T. Yang, X. Guo, S. Wu, S. Wang, S. Zhang, Nanotechnology. 22 (2011) 185501-185508.

[13] S.K. Sahoo, M. Mohapatra, B. Pandey, Mater. Characterization. 60 (2009) 425.-431.

[14] M.X. Liu, Y.S. Fu, M.H. Xiao, J.C. Huang, J. Solid State Chem. 178 (2005) 2798.-2803.

[15] S. Giri, S. Samanta, S. Maji, S. Ganguli, A. Bhaumik, J. Magn. Magn. Mater. 285 (2005) 296.-302.

[16] H. Wang, G. Wang-Chang, Res Chem Intermed. 37 (2011) 523-529.

[17] P.T. Raming, A.J.A. Winnubst, C.M. Van Kats, P.A. Philipse, J. Colloid Interface Sci. 249 (2002) 346.-350.

[18] Y.S. Koo, B.K. Yun, J.H. Jung, J. Magnetics. 15 (2010) 21-24.

[19] X.Q. Liu, S.W. Tao, Y.S. Shen, Sens Actuators B. 40 (1997) 161–165.

[20] A.B. Chin, I.I. Yaacob, J Mater Process Tech. 191 (2007), 235–237.

[21] S.U. Sonavane, M.B. Gawande, S.S. Deshpande, A. Venkataraman, R.V. Jayaram, Catal Commun. 8 (2007) 1803–1806.

[22] S. Chaianansutcharit, O. Mekasuwandumrong, P. Praserthdam, Ceram Int. 33 (2007) 697–699.

[23] C.Q. Hu, Z.H. Gao, X.R. Yang, Mater Chem Phys. 104 (2007) 429–433.

[24] B. Wang, Q. Wei, S. Qu, Int. J. Electrochem. Sci. 8 (2013) 3786-3793.